IEEE Access
Multidisciplinary ⋮ Rapid Review ⋮ Open Access Journal

Received 8 February 2023, accepted 1 March 2023, date of publication 6 March 2023, date of current version 14 March 2023.

Digital Object Identifier 10.1109/ACCESS.2023.3253506

RESEARCH ARTICLE

Setting Free Fault Location for Three-Terminal Hybrid Transmission Lines Connected With Conventional and Renewable Resources

KUKKALA LIKHITHA AND O. D. NAIDU, (Senior Member, IEEE)
Hitachi Energy Grid Automation, Bengaluru, Karnataka 560048, India
Corresponding author: Kukkala Likhitha (kukkala.likhitha@hitachienergy.com)

ABSTRACT Three-terminal hybrid transmission lines (TTHTLs) are attractive from both environmental and commercial view. Hybrid transmission lines are growing due to urbanization, connecting an industrial load and renewable integration. A TTHTL comprises sections of both overhead lines and underground/subsea cables or overhead lines with different X/R ratios. Faulted section identification (FSI) is key for defining the adaptive/selective auto-reclosing scheme and estimation of the fault location for TTHTLs. In this paper, FSI and fault location algorithms are proposed without using the parameters of any line section. Novelty of the methodology lies in a two-stage approach to the problem. In the first stage, series impedance parameters of all the sections are calculated using closed loop formulae. These parameters are then utilized in identifying the faulted section. In the second stage, the above calculated line section parameters and faulted section are used to estimate complete line parameters including shunt capacitance and subsequently the fault location. The advantage of the proposed method is that it does not require an initial guess of the line section parameters, is non-iterative in the first stage, and provides correct fault section identification for TTHTLs. These features make it suitable for designing the selective auto-reclosing protection scheme for the TTHTLs within traditional protection relaying hardware. More importantly, the series impedance parameters calculated in the first stage constitute good initialization values for the non-linear problem of estimating the complete line parameters. This results in better convergence of the algorithm and accurate parameter estimation. The developed solution is verified using the PSCAD/EMTDC simulations for TTHTLs connected with conventional and different inverter-based renewable resources. The performance of the proposed solution is compared with commercially available solutions, and it is found to be accurate. This solution is amenable for implementation in line differential protection relays without additional infrastructural changes.

INDEX TERMS Adaptive auto-reclosing protection scheme, inverter-based renewable resources, faulted section identification, fault location, parameter estimation, three-terminal hybrid transmission lines.

NOMENCLATURE

A. VARIABLES

V_S^{1pre}, V_R^{1pre}, V_T^{1pre}	positive sequence pre-fault voltages measured at terminal S, R, and T respectively.
I_S^{1pre}, I_R^{1pre}, I_T^{1pre}	positive sequence pre-fault currents measured at terminals S, R, and T respectively.
V_S^{1f}, V_R^{1f}, V_T^{1f}	positive sequence during fault voltages measured at terminal S, R, and T respectively.
I_S^{1f}, I_R^{1f}, I_T^{1f}	positive sequence during fault currents measured at terminals S, R, and T respectively.
Z_{SJ}^1, Z_{RJ}^1 and Z_{TJ}^1	positive sequence impedance of section SJ, RJ and TJ respectively in per km.
R_{SJ}^1, R_{RJ}^1 and R_{TJ}^1	positive sequence resistance of section SJ, RJ and TJ respectively in per km.

The associate editor coordinating the review of this manuscript and approving it for publication was Sarasij Das.

L^1_{SJ}, L^1_{RJ} and L^1_{TJ}	positive sequence inductance of section SJ, RJ and TJ respectively in per km.
Y^1_{SJ}, Y^1_{RJ} and Y^1_{TJ}	positive sequence admittance of section SJ, RJ and TJ respectively in per km.
C^1_{SJ}, C^1_{RJ} and C^1_{TJ}	positive sequence capacitance of section SJ, RJ and TJ respectively in per km.
Z^1_{chSJ}, Z^1_{chRJ}, Z^1_{chTJ}	positive sequence characteristic impedance of section SJ, RJ and TJ respectively.
γ^1_{SJ}, γ^1_{RJ}, γ^1_{TJ}	positive sequence propagation constant of section SJ, RJ, and TJ respectively.
$(ABCD)^1_X$	ABCD parameters of each section (X=SJ, RJ, TJ).
l_{SJ}, l_{RJ}, l_{TJ}	length of section SJ, RJ, and TJ respectively.

B. ABBREVIATIONS

TTHTLs	Three-Terminal Hybrid Transmission Lines.
FSI	Faulted Section Identification.
AARPS	Adaptive Auto-Reclosing Protection Scheme.
ARPS	Auto-Reclosing Protection Scheme.
OHL	Overhead Line.
UGC	Underground Cable.
SC	Subsea Cable.
FL	Fault Location.
PE	Parameter Estimation.
TW	Traveling Wave.
IBR	Inverter Based Renewable Resources.
AI	Artificial Intelligence.
ML	Machine Learning.
TTL	Three Terminal Lines.
SCADA	Supervisory Control and Data Acquisition.
PMU	Phasor Measurement Unit.
IED	Intelligent Electronic Device.

I. INTRODUCTION

A. MOTIVATION

In recent years, several three-terminal hybrid transmission lines (also known as non-homogeneous or mixed) are growing in modern power systems due to urbanization, connecting industrial loads, and renewable integration with minimum cost. A hybrid transmission line comprises sections of both OHL and UGC/SC or OHL with different X/R ratios, to connect offshore wind farms to existing lines, and mitigate right-of-way related issues in urban areas [1]. This reduces the installation and maintenance costs for a substation and costs related to the measurement transformers and breaker equipment [2]. The distance protection of such configurations is challenging due to the current infeed and outfeed, and different X/R ratios [3], [4] of each section. Current infeed and outfeed are conditions where the current contribution from a line terminal can cause a distance relay to underreach or overreach [3], [4]. To mitigate these protection issues, the line differential is a common protection scheme employed for three-terminal hybrid lines [5], [6], [7]. However, fault section identification, fault location, and parameter estimation are highly challenging as the line sections have different surge impedance and line propagation constants. This paper focus on (i) fault section identification, (ii) fault location, and (iii) parameter estimation of the three-terminal hybrid lines.

B. LITERATURE REVIEW

Auto-reclosing (AR) is very important for the reliability of the power system [8]. CIGRE report [9] defines accepted practices for ARPS and what is to be practiced in special cases like three-terminal hybrid lines. ARPS is enabled for overhead lines since most faults are transient, but it is blocked for underground/subsea cables because most of the cable faults are permanent. The guidelines specify that ARPS should be used on hybrid lines only if the faulted section is known [9]. For three-terminal hybrid lines, FS identification is challenging since the parameters such as resistance, inductance is different for each section. Traveling wave [10], [11], [12] and AI/ML [13], [14] based faulted section identification methods are proposed for hybrid lines. TW based methods require high sampling hardware and communication and it is not a cost-effective solution. Even though AI/ML technology has gained attention in recent literature, the model generality is a challenge, and it requires a longer time to mature and for practical deployment of these solutions.

Impedance-based fault section identification methods are proposed for two-terminal [15] and three-terminal [16] hybrid lines. The accuracy of these methods depends on each section's electrical parameters and these parameters change with the temperature and aging of the conductors, especially for UGC/SC sections. A setting-free fault section identification is proposed in [17]. This method requires the negative sequence network equations which may not be available for lines connected with IBRs [18], [19], [20]. Therefore, there is a requirement for a reliable *setting-free* FSI algorithm for TTHTLs which is used for ARPS and fault location estimation.

Locating the fault on the line is important to expedite the power supply restoration [21]. For quick restoration of faulted transmission lines, an exact FL must be known, else, the maintenance job becomes tiresome and takes a lot of time for power networks spread in rugged geographical terrains [22]. Thus, accurate FL in transmission lines is crucial for the outage management team to reach the fault point and start repair at the earliest. Several TW [23], [24], [25] and impedance-based [26], [27], [28] algorithms are proposed for two-terminal lines. However, these algorithms cannot be extended directly to three-terminal hybrid lines, as the impedance of each section is not uniform, and different infeed/outfeed of the current lead to more errors in the fault location estimation [28], [29]. Many fault location algorithms traveling wave based [30], [31], AI/ML [13], [14], and

impedance-based [32], [33], [34], [35], [36], [37], [38], [39], [40] are presented for three-terminal lines including hybrid lines. TW-based methods [30], [31] require each section's wave speed as an input, which is not easy to get in a real-world implementation. Moreover, traveling wave-based methods provide higher accuracy, but it requires high sampling rates and more communication bandwidth which adds to the cost. Although the application of AI/ML in the field of power system monitoring is maturing, for power system protection and fault location applications it may not be practical, as it requires abundant practical or simulated data to train and build the accurate and generic AI/ML models.

Fault location using fundamental phasors are widely used because of their ease of use, low sampling rate data requirement, communication bandwidth, and low hardware cost. Depending on the measurements required, they are classified into single-ended and multi-ended methods [21], [22]. Single-ended methods [26], [27] are easy to implement as it does not require any communication link or data synchronization. However, the accuracy of FL greatly varies with system non-homogeneity, fault resistance, and fault information [28], [29]. These methods will pose larger fault location errors for lines connected with IBRs [20], as the renewable connected systems introduce larger deviations in phase angles of the local and remote currents [19]. Therefore, the performance of the single-ended approaches is limited for extending to the three-terminal hybrid lines due to the infeed/outfeed at the tap point and IBR connections. The fault location for three-terminal double circuit lines is presented using single-ended data and requires line parameters as a setting [32]. The method uses negative sequence quantities to obtain the fault location.

To mitigate the issues of single-ended FL methods, several multi-ended fault location methods [33], [34], [35], [36], [37], [38], [39], [40] for three-terminal lines including hybrid lines are developed. A negative sequence magnitude-based method is proposed in [33] which does not require data synchronization. The FL accuracy does not depend on the pre-fault load, and it is commercially available. The method in [34] computes fault location using the two-ends data of a three-terminal line, the third terminal being connected to renewable energy sources (RES) using positive and negative sequence quantities. It requires line parameters as input. These lines parameters are varying due to changes in temperature, aging, the sag of the conductor, etc., of the line and this would affect the accuracy of the fault location. However, the methods [32], [33], [34] may not work for all faults as there are no negative sequence currents for balanced faults. Moreover, this method will not work for lines connected with inverter-based renewable resources as most of the grid codes will not supply negative sequence currents [18], [19]. And also, require line parameters as a setting. Fault location using only two end measurements [35] and three-terminal current measurements [36] are proposed for three-terminal lines. These methods require the source impedance and fault loop as inputs which is difficult for renewable connected systems. The source impedance of the inverter-based resource continuously varies during the fault [19] and it may lead to larger deviation in fault location calculation. The proposed solutions may not work well for networks connected with IBRs. Positive sequence voltage and current-based FL approaches for TTLs are proposed in [37] and [38]. These methods are designed for only homogeneous three-terminal lines and the accuracy of these methods highly depends on the parameters of each section. In [39], proposed a new FSI and FL solution based on synchronized data from all ends of three-terminal lines. In the absence of data synchronization, it calculates the value of synchronization operators to form a common reference among the all-end data and accuracy depends on the line parameters. In [40], a new phasor-based technique is proposed to locate faults in non-homogeneous/hybrid transmission lines using synchronized data from all ends. This method uses state estimation to solve the fault location and they require the impedance matrixes of the OHL and UGC sections. Though several methods are reported in the literature, the accuracy of the reported fault location algorithms depends on the precision of each section parameters. The electrical parameters such as resistance, inductance, and capacitance of an electrical line are not known with great precision. Many case studies show that actual and stored values of the electrical parameters of the lines can differ by up to 25–30% [41], especially for UGC section parameters. Line parameter with decent precision is enough for monitoring and protection functions but for precise FL, accurate line electrical parameters are essential. These electrical parameters of each section of TTHTLs are not constant and vary with many weather/seasonal situations including the age of the transmission line/cables, etc.

The estimation of electrical parameters of each section will improve the reliability of the FSI and precision of FL for TTHTLs. Line parameter estimation methods for two-terminal homogeneous transmission lines using a single set [42], [43] and multiple sets [44], [45] are presented. These methods cannot be applied to the three-terminal hybrid lines, as each section has different parameters and outfeed/infeed at the junction point. A technique [46] is presented for the estimation of each section electrical parameters for multi-terminal lines while the required data are phasor measurements at one end of a given line and conventional magnitude measurements at the other end. The presented solution is thus based on combining the PMU and SCADA measurements. A non-linear weighted least-square error (NWLSE) algorithm is employed for the maximum-likelihood estimation of parameters. This may not work for hybrid three-terminal lines. To mitigate the need for several data sets, a technique to determine the parameters for TTHTLs using pre and during-fault signals is presented in [47] and [48]. The method in [47] uses positive sequence quantities to obtain the fault location along with the line parameters using the trust region optimization algorithm. Implementation of such a high computational

method in the IED platform is difficult. The success of the method depends on the proper initial guess. The method in [48] requires positive and negative sequence quantities, it may not work when IBRs are connected in the network. These techniques need proper initial guess. The literature review indicates that there is a scope for research in FSI and FL for three-terminal hybrid transmission lines without using any settings.

C. CONTRIBUTIONS

In this paper, a *setting-free* faulted section identification and fault location method for three-terminal hybrid transmission lines connected with conventional/renewable resources using multi-ended voltage and current signals are proposed. The method calculates the series impedance of each section by closed-loop formulae using all terminal pre-fault data. The faulted section is identified by comparing the calculated and measured voltage at each terminal using the calculated series impedance parameters (resistance and inductance) and during fault data. This process does not require any complex iterative computations to identify the faulted section of the hybrid transmission lines. Therefore, the identified faulted section information can be used for a selective auto-reclosing protection scheme (i.e., block for fault in UGC and enable for fault in OHL) for these hybrid three-terminal lines. The complete parameters including shunt capacitance are obtained by using pre-fault data, using series impedance calculated in the previous step as an initial guess. As a final step, accurate FL is computed using the estimated electrical constants/parameters of each section, faulted section identification information, and fault data.

The developed solution does not require any user settings and reduces the practical deployment time and maintenance cost. The main contributions of this paper are as follows:

- A method for fault location on hybrid three-terminal transmission line which does not require line parameters to be provided as an input.
- Solution to estimate parameters of the distributed parameter (long line corrected equivalent pi) model of the line, using a single set of voltage and current data, and not requiring any initial values of the parameters as an input or user setting. The initial values are instead calculated through closed loop formulae based on a simplistic RL model of the line.
- The proposed methodology is deployable in conventional and renewable connected transmission systems.

The developed solution is tested for various fault scenarios using PSCAD/EMTDC for 220-kV, 120km main OHL, and 20km UGC connected with conventional generations/IBRs. The simulation results are reliable, and the proposed solution is able to identify the faulted section reliably and determine the distance to the fault within a 300 - 600 m (two-tower span) distance, using low sampling (1kHz sampling) signals. The proposed FSI and FL methods are implemented in the existing IED/relay platform [7], and it is an economical alternative for multi-ended TW-based methods. Since the proposed method is achieved using the existing hardware of the IED, there is no additional cost involved. Further, communication between the three ends does not require a dedicated communication channel. Data is exchanged over IEEE C37.94 protocol and can be shared over a multiplexed communication channel using Synchronous Digital Hierarchy (SDH) supporting a bandwidth of 2 Mbps. This does not incur any additional cost for the proposed method, as such communication is essential for working on existing line differential protection IEDs. Since it does not require additional settings or commissioning to put it in operation, it is practically free of any deployment and overhead costs. Moreover, this algorithm provides parameters for each section, and those parameters can be used for other protection and monitoring applications.

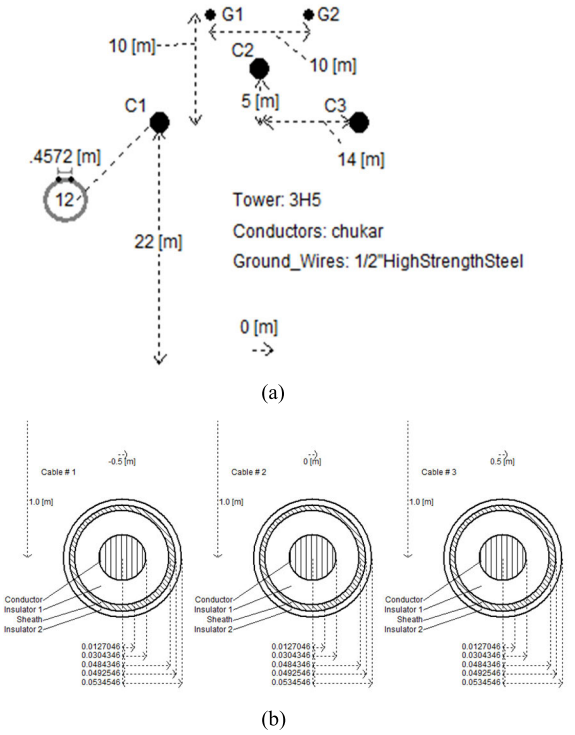

FIGURE 1. Shows the geometry of the (a) overhead transmission line and (b) underground cable, used in the simulation.

II. PROPOSED METHOD

The transmission line is simulated using a frequency-dependent phase model as shown in Fig. 1, which is the most realistic representation of a transmission line in simulations. However, in our solution approach, in the first stage, we map the measurements to a series RL (lumped parameter) model of the line, to avoid complexity. The outcome of this step are the estimates of the lumped parameters R and L. In the next stage, we use these estimates as an initial guess to determine the parameters namely, characteristic impedance (Z_{ch}) and propagation constant (γ) of the distributed parameter (long line corrected equivalent pi) model as shown in Fig. 6.

This approach will eliminate the requirement of multiple data sets and initial guess of parameters Z_{ch} and γ to solve the non-linear equations that arise in the scenario when we directly try to map measurements on to the model of Fig. 6. This approach is simple, requires less computations and easy to implement in the existing relay platform. The proposed method uses four modules: (A) setting-free faulted section identification, (B) calculation of line series impedance, (C) estimation of line parameters using distributed model, and (D) fault location. The details are provided below.

A. FAULTED SECTION IDENTIFICATION METHOD

This section represents the method of identifying faulted section using the series impedance of lumped model. Let us consider TTHTLs connected with conventional or inverter-based resources as shown in Fig. 2.

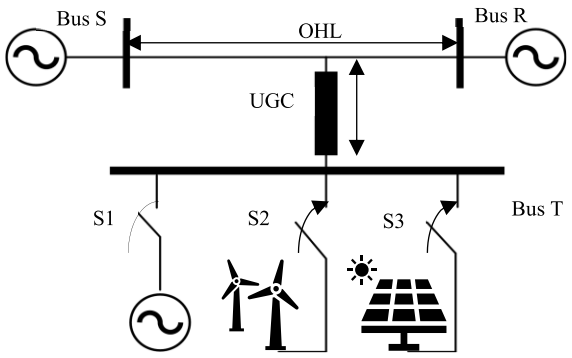

FIGURE 2. Three-terminal networks connected to conventional or renewable power plants.

Consider fault on the SJ section at a distance from the fault of d_{SJ} from Bus S as shown in Fig. 3. Positive sequence voltage at Bus S is determined using positive sequence current and voltage from Bus R and current from Bus S.

Calculate the junction voltage V_{JR}^{1f} using Bus R voltage, current, and impedance parameters, as in (1)

$$V_{JR}^{1f} = V_R^{1f} - I_R^{1f} Z_{RJ}^1 l_{RJ} \tag{1}$$

Now, using the Bus S current, section SJ impedance parameters, and estimated junction voltage, compute terminal S voltage.

$$V_{Scalc}^{1f} = V_{JR}^{1f} \mathcal{C} I_S^{1f} Z_{SJ}^1 l_{SJ} \tag{2}$$

By substituting equation (1) in (2), we get (3)

$$V_{Scalc}^{1f} = V_R^{1f} - I_R^{1f} Z_{RJ}^1 l_{RJ} \mathcal{C} I_S^{1f} Z_{SJ}^1 l_{SJ} \tag{3}$$

Similarly, voltage at Bus R is determined using current and voltage measured at Bus T, current measured at Bus R, and positive sequence parameters of section RJ, as in (4)

$$V_{Rcalc}^{1f} = V_T^{1f} - I_T^{1f} Z_{TJ}^1 l_{TJ} + I_R^{1f} Z_{RJ}^1 l_{RJ} \tag{4}$$

Finally, voltage at Bus T is determined using current and voltage measured at Bus S, current measured at Bus T, and

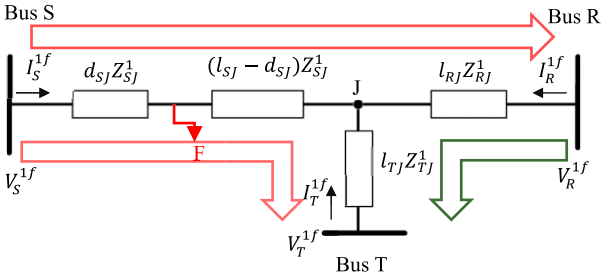

FIGURE 3. During fault lumped equivalent model of TTHTLs.

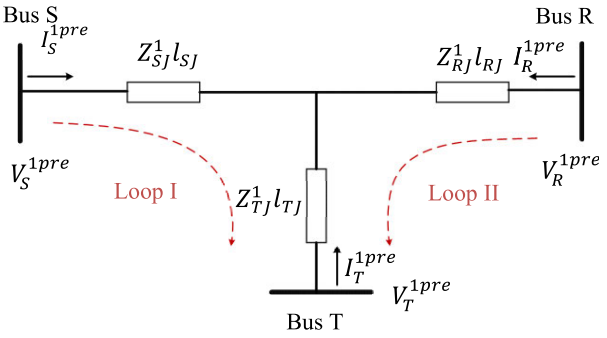

FIGURE 4. Pre-fault equivalent model of three-terminal lumped model.

positive sequence parameters of section TJ, as in (5),

$$V_{Tcalc}^{1f} = V_S^{1f} - I_S^{1f} Z_{SJ}^1 l_{SJ} + I_T^{1f} Z_{TJ}^1 l_{TJ} \tag{5}$$

Compute the deviation of calculated voltage from the measured voltage at each terminal, as in (6) to (8)

$$\Delta V_{SR} = \left| V_{Scalc}^{1f} - V_S^{1f} \right| \tag{6}$$

$$\Delta V_{RT} = \left| V_{Rcalc}^{1f} - V_R^{1f} \right| \tag{7}$$

$$\Delta V_{TS} = \left| V_{Tcalc}^{1f} - V_T^{1f} \right| \tag{8}$$

The minimum the deviation of the calculated voltage from the measured voltage at each terminal indicates that the sections involved in the computation of the calculated voltage are healthy, concluding that the fault is in another section (in this case-section TJ and RJ are healthy as marked in green in Fig. 3).

The proposed faulted section identification method is summarized as follows,

- If ΔV_{SR}, ΔV_{RT}, and ΔV_{TS} $<\in$, then the fault is at the junction.
- If ΔV_{RT} is minimum of ΔV_{SR}, ΔV_{RT}, and ΔV_{TS}, then the fault is in the SJ section.
- If ΔV_{TS} is minimum of ΔV_{SR}, ΔV_{RT}, and ΔV_{TS}, then the fault is in the RJ section.
- If ΔV_{SR} is minimum of ΔV_{SR}, ΔV_{RT}, and ΔV_{TS}, then the fault is in the TJ section.

The accuracy of identifying the faulted section depends on the series impedance parameters of each section, which are obtained using pre-fault current and voltage phasors in a closed-loop formulae and details are provided in section B.

B. CALCULATION OF SERIES IMPEDANCE PARAMETERS IN CLOSED LOOP FORMULAE

This section presents a closed loop series impedance parameters calculation for TTHTLs with at least one section having a different set of parameters. Consider R-L model as shown in Fig. 4. From Fig. 4, KVL across loop I is given as

$$V_S^{1pre} - I_S^{1pre} Z_{SJ}^1 l_{SJ} - \left(I_S^{1pre} + I_R^{1pre}\right) Z_{TJ}^1 l_{TJ} - V_T^{1pre} = 0 \tag{9}$$

KVL across loop II is given as

$$V_R^{1pre} - I_R^{1pre} Z_{RJ}^1 l_{RJ} - \left(I_S^{1pre} + I_R^{1pre}\right) Z_{TJ}^1 l_{TJ} - V_T^{1pre} = 0 \tag{10}$$

It is assumed that the main section has the same parameters which are different from the tapped line, i.e, $Z_{SJ}^1 = Z_{RJ}^1$.

From equations (9) and (10), Z_{SJ}^1 is calculated as in (11)

$$Z_{SJ}^1 = \frac{V_S^{1pre} - V_R^{1pre}}{I_S^{1pre} l_{SJ} - I_R^{1pre} l_{RJ}} \tag{11}$$

By substituting Z_{SJ}^1 in (1), Z_{TJ}^1 is calculated as in (12)

$$Z_{TJ}^1 = \frac{V_S^{1pre} - I_S^{1pre} Z_{SJ}^1 l_{SJ} - V_T^{1pre}}{\left(I_S^{1pre} + I_R^{1pre}\right) l_{TJ}} \tag{12}$$

The calculated series impedances are used to identify the faulted section described in section -A. The series impedance is also used as an initial guess for the complete parameter estimation method described in section D.

C. FAULT LOCATION METHOD FORMULATION

This section presents the method of obtaining distance to fault for hybrid three-terminal lines. The formulation of fault location [37] is obtained by equating the voltage at the fault point determined from both terminals of the faulted section. The detailed steps are as follows.

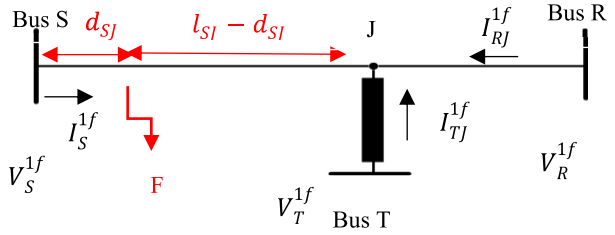

FIGURE 5. A-g fault on SJ section for a TTHTLs.

Consider fault on SJ section at a distance of d_{SJ} from Bus S as shown in Fig. 5 and corresponding pre and during fault network equivalent are shown in Fig. 6 and Fig. 7 respectively. Calculate the current flowing towards the junction from both the healthy sections. The current flowing towards the junction

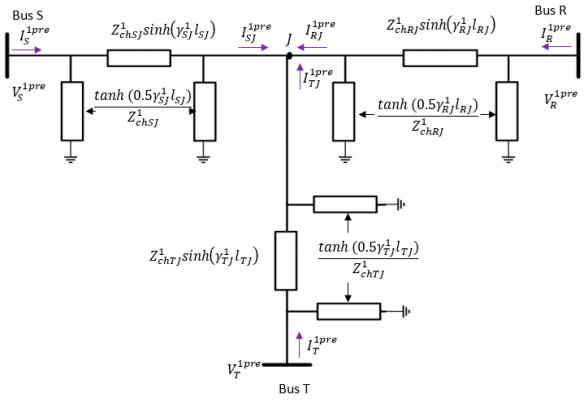

FIGURE 6. Pre-fault distributed parameter model (long line corrected equivalent pi model).

from Bus R and T is given in (13) and (14)

$$I_{RJ}^{1f} = -C_{RJ}^1 V_R^{1f} + A_{RJ}^1 I_R^{1f} \tag{13}$$

$$I_{TJ}^{1f} = -C_{TJ}^1 V_T^{1f} + A_{TJ}^1 I_T^{1f} \tag{14}$$

From (13) and (14), the current flowing towards the fault point from the junction is given by (15)

$$I_J^{1f} = I_{RJ}^{1f} + I_{TJ}^{1f} \tag{15}$$

Determine the junction voltage from both the healthy terminals

$$V_{RJ}^{1f} = D_{RJ}^1 V_R^{1f} - B_{RJ}^1 I_R^{1f} \tag{16}$$

$$V_{TJ}^{1f} = D_{TJ}^1 V_T^{1f} - B_{TJ}^1 I_T^{1f} \tag{17}$$

The junction voltage is taken as the average value

$$V_J^{1f} = \frac{V_{RJ}^{1f} + V_{TJ}^{1f}}{2} \tag{18}$$

where

$$Z_{chRJ}^1 = \sqrt{\frac{Z_{RJ}^1}{Y_{RJ}^1}} = \sqrt{\frac{R_{RJ}^1 + j\omega L_{RJ}^1}{j\omega C_{RJ}^1}};$$

$$\gamma_{RJ}^1 = \sqrt{Z_{RJ}^1 Y_{RJ}^1} = \sqrt{(R_{RJ}^1 + j\omega L_{RJ}^1)(j\omega C_{RJ}^1)};$$

$$A_{RJ}^1 = D_{RJ}^1 = \cosh\left(\gamma_{RJ}^1 l_{RJ}\right); B_{RJ}^1 = Z_{chRJ}^1 \sinh\left(\gamma_{RJ}^1 l_{RJ}\right);$$

$$C_{RJ}^1 = \frac{\sinh\left(\gamma_{RJ}^1 l_{RJ}\right)}{Z_{chRJ}^1};$$

$(ABCD)_{RJ}^1$ are ABCD parameters of section RJ

$$Z_{chTJ}^1 = \sqrt{\frac{Z_{TJ}^1}{Y_{TJ}^1}} = \sqrt{\frac{R_{TJ}^1 + j\omega L_{TJ}^1}{j\omega C_{TJ}^1}};$$

$$\gamma_{TJ}^1 = \sqrt{Z_{TJ}^1 Y_{TJ}^1} = \sqrt{(R_{TJ}^1 + j\omega L_{TJ}^1)(j\omega C_{TJ}^1)};$$

$$A_{TJ}^1 = D_{TJ}^1 = \cosh\left(\gamma_{TJ}^1 l_{TJ}\right); B_{TJ}^1 = Z_{chTJ}^1 sinh\left(\gamma_{TJ}^1 l_{TJ}\right);$$

$$C_{TJ}^1 = \frac{\sinh\left(\gamma_{TJ}^1 l_{TJ}\right)}{Z_{chTJ}^1};$$

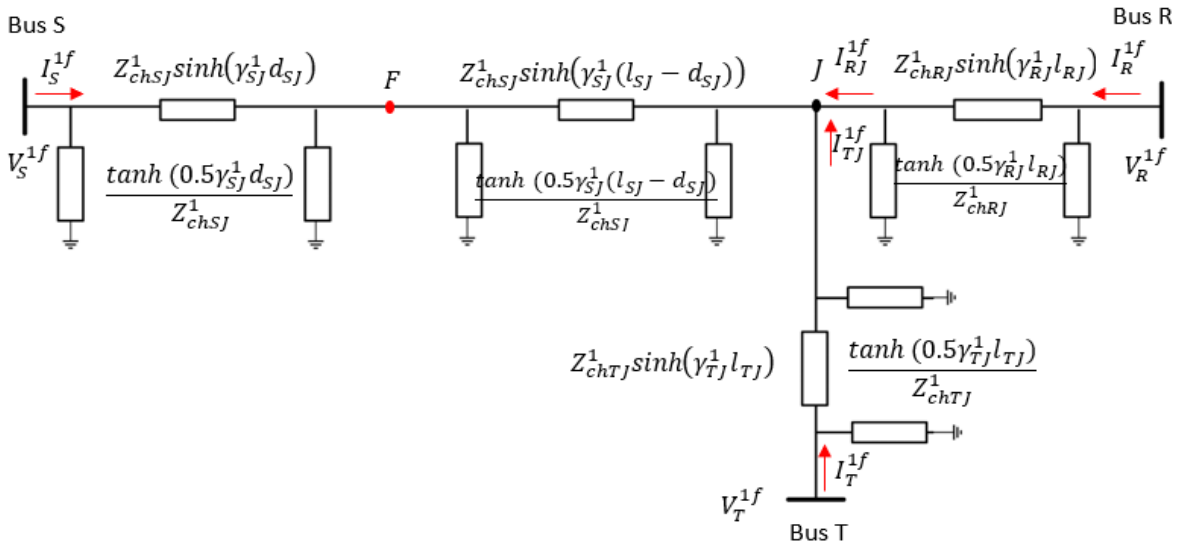

FIGURE 7. During fault distributed parameter model for fault in section SJ at a distance of d_{SJ} from Bus S.

$(ABCD)^1_{TJ}$ are ABCD parameters of section TJ

Determine voltage at the fault point using current and voltage measured from Bus S

$$V^{1f}_{SF} = D^1_{d_{SJ}} V^{1f}_S - B^1_{d_{SJ}} I^{1f}_S \tag{19}$$

Determine voltage at the fault point using current and voltage measurements obtained at the junction from previous steps

$$V^{1f}_{JF} = D^1_{l_{SJ}-d_{SJ}} V^{1f}_J - B^1_{l_{SJ}-d_{SJ}} I^{1f}_J \tag{20}$$

where

$$Z^1_{chSJ} = \sqrt{\frac{Z^1_{SJ}}{Y^1_{SJ}}} = \sqrt{\frac{R^1_{SJ} + j\omega L^1_{SJ}}{j\omega C^1_{SJ}}};$$
$$\gamma^1_{SJ} = \sqrt{Z^1_{SJ} Y^1_{SJ}} = \sqrt{(R^1_{SJ} + j\omega L^1_{SJ})(j\omega C^1_{SJ})}$$
$$A^1_{d_{SJ}} = D^1_{d_{SJ}} = \cosh\left(\gamma^1_{SJ} d_{SJ}\right); B^1_{d_{SJ}} = Z^1_{chSJ} \sinh\left(\gamma^1_{SJ} d_{SJ}\right);$$
$$C^1_{d_{SJ}} = \frac{\sinh\left(\gamma^1_{SJ} d_{SJ}\right)}{Z^1_{chSJ}};$$

$(ABCD)^1_{d_{SJ}}$ are ABCD parameters of the section, from Bus S to the fault point

$$A^1_{l_{SJ}-d_{SJ}} = D^1_{l_{SJ}-d_{SJ}} = \cosh\left(\gamma^1_{SJ}(l_{SJ} - d_{SJ})\right);$$
$$B^1_{l_{SJ}-d_{SJ}} = Z_{chSJ} \sinh\left(\gamma^1_{SJ}(l_{SJ} - d_{SJ})\right);$$
$$C^1_{l_{SJ}-d_{SJ}} = \frac{\sinh\left(\gamma^1_{SJ}(l_{SJ} - d_{SJ})\right)}{Z^1_{chSJ}};$$

$(ABCD)^1_{l_{SJ}-d_{SJ}}$ are ABCD parameters of the section, from fault point to the junction

By equating the voltage at the fault point when calculated from Bus S and Junction, we obtain the unknown fault location as in (21)

$$d_{SJ} = \frac{1}{\gamma^1_{SJ}} \tanh^{-1}\left(\frac{K1}{K2}\right) \tag{21}$$

The inverse hyperbolic tangent cannot be implemented in IED platforms directly; therefore equation (21) can be further simplified as shown in equation (22) which will be easy to implement.

$$d_{SJ} = \frac{0.5}{\gamma^1_{SJ}} \left(\ln\left(1 + \frac{K1}{K2}\right) - \ln\left(1 - \frac{K1}{K2}\right)\right) \tag{22}$$

where,

$$K1 = V^{1f}_S - D^1_{SJ} D^1_{RJ} V^{1f}_R + D^1_{SJ} B^1_{RJ} I^{1f}_R - B^1_{SJ} C^1_{RJ} V^{1f}_R + B^1_{SJ} A^1_{RJ} I^{1f}_R - B^1_{SJ} C^1_{TJ} V^{1f}_T + B^1_{SJ} A^1_{TJ} I^{1f}_T \tag{23}$$

$$K2 = Z^1_{chSJ}(I^{1f}_S - C^1_{SJ} D^1_{RJ} V^{1f}_R + C^1_{SJ} B^1_{RJ} I^{1f}_R - D^1_{SJ} C^1_{RJ} V^{1f}_R + D^1_{SJ} A^1_{RJ} I^{1f}_R - D^1_{SJ} C^1_{TJ} V^{1f}_T + D^1_{SJ} A^1_{TJ} I^{1f}_T) \tag{24}$$

Similarly, for fault in the RJ section at a distance of d_{RJ} from Bus R, the unknown fault location d_{RJ} is obtained as in (25),

$$d_{RJ} = \frac{0.5}{\gamma^1_{RJ}} \left(\ln\left(1 + \frac{K1}{K2}\right) - \ln\left(1 - \frac{K1}{K2}\right)\right) \tag{25}$$

where,

$$K1 = V^{1f}_R - D^1_{RJ} D^1_{SJ} V^{1f}_S + D^1_{RJ} B^1_{SJ} I^{1f}_S - B^1_{RJ} C^1_{SJ} V^{1f}_S + B^1_{RJ} A^1_{SJ} I^{1f}_S - B^1_{RJ} C^1_{TJ} V^{1f}_T + B^1_{RJ} A^1_{TJ} I^{1f}_T \tag{26}$$

$$K2 = Z^1_{chRJ} * \left(I^{1f}_R - C^1_{RJ} D^1_{SJ} V^{1f}_S + C^1_{RJ} B^1_{SJ} I^{1f}_S - D^1_{RJ} C^1_{SJ} V^{1f}_S + D^1_{RJ} A^1_{SJ} I^{1f}_S - D^1_{RJ} C^1_{TJ} V^{1f}_T + D^1_{RJ} A^1_{TJ} I^{1f}_T\right) \tag{27}$$

Similarly, for fault in the TJ section at a distance of d_{TJ} from Bus T, the unknown fault location d_{TJ} is obtained as in (28),

$$d_{TJ} = \frac{0.5}{\gamma^1_{TJ}} \left(\ln\left(1 + \frac{K1}{K2}\right) - \ln\left(1 - \frac{K1}{K2}\right)\right) \tag{28}$$

where,

$$\begin{aligned} K1 = {} & V_T^{1f} - D^1_{TJ} D^1_{SJ} V_S^{1f} + D^1_{TJ} B^1_{SJ} I_S^{1f} \\ & - B^1_{TJ} C^1_{SJ} V_S^{1f} + B^1_{TJ} A^1_{SJ} I_S^{1f} \\ & - B^1_{TJ} C^1_{RJ} V_R^{1f} + B^1_{TJ} A^1_{RJ} I_R^{1f} \end{aligned} \tag{29}$$

$$\begin{aligned} K2 = {} & Z^1_{chTJ} * \left(I_T^{1f} - C^1_{TJ} D^1_{SJ} V_S^{1f} + C^1_{TJ} B^1_{SJ} I_S^{1f} \right. \\ & - D^1_{TJ} C^1_{SJ} V_S^{1f} + D^1_{TJ} A^1_{SJ} I_S^{1f} \\ & \left. - D^1_{TJ} C^1_{RJ} V_R^{1f} + D^1_{TJ} A^1_{RJ} I_R^{1f} \right) \end{aligned} \tag{30}$$

The fault location obtained for each section requires line parameters including capacitance of the three-terminal hybrid transmission line. The required line parameters are estimated using the pre-fault data in section D.

D. ESTIMATION OF COMPLETE LINE PARAMETERS

In this section, the parameter estimation formulae are derived using pre-fault network equivalent as shown in Fig. 6. The objective functions are formulated as follows:

By equating junction voltage when calculated from Bus S and T measurements, we get F_I as

$$F_I = D^1_{SJ} V_S^{1pre} - B^1_{SJ} I_S^{1pre} - D^1_{TJ} V_T^{1pre} + B^1_{TJ} I_T^{1pre} = 0 \tag{31}$$

Similarly, by equating junction voltage when calculated from Bus R and T measurements, we get F_{II} as

$$F_{II} = D^1_{RJ} V_R^{1pre} - B^1_{RJ} I_R^{1pre} - D^1_{TJ} V_T^{1pre} + B^1_{TJ} I_T^{1pre} = 0 \tag{32}$$

Finally, by applying KCL at the junction, we get F_{III} as

$$\begin{aligned} F_{III} = {} & C^1_{SJ} V_S^{1pre} - A^1_{SJ} I_S^{1pre} + C^1_{RJ} V_R^{1pre} - A^1_{RJ} I_R^{1pre} \\ & + C^1_{TJ} V_T^{1pre} - A^1_{TJ} I_T^{1pre} = 0 \end{aligned} \tag{33}$$

where

$$A^1_{SJ} = D^1_{SJ} = \cosh\left(\gamma^1_{SJ} l_{SJ}\right); B^1_{SJ} = Z^1_{chSJ} \sinh\left(\gamma^1_{SJ} l_{SJ}\right);$$

$$C^1_{SJ} = \frac{\sinh\left(\gamma^1_{SJ} l_{SJ}\right))}{Z^1_{chSJ}};$$

$(ABCD)^1_{SJ}$ are ABCD parameters of section SJ.

There are a total of six unknowns to be estimated.

$$X = \left(R^1_{SJ}, L^1_{SJ}, C^1_{SJ}, R^1_{TJ}, L^1_{TJ}, C^1_{TJ}\right)^T$$

The objective functions are further split into real and imaginary parts.

$$\left.\begin{aligned} f_1(X) &= Re(F_I) \\ f_2(X) &= Im(F_I) \\ f_3(X) &= Re(F_{II}) \\ f_4(X) &= Im(F_{II}) \\ f_5(X) &= Re(F_{III}) \\ f_6(X) &= Im(F_{III}) \end{aligned}\right\} \tag{34}$$

The non-linear objective functions are solved using the least-squares iterative method, with an initial guess as calculated in section -B,

$$X_0 = \left(R^1_{SJ}, L^1_{SJ}, 1.5C^1_{SJ}, R^1_{TJ}, L^1_{TJ}, 1.5C^1_{TJ}\right)^T$$

This results in better convergence of the algorithm and accurate parameter estimation. These estimated parameters are used to calculate precise fault location as formulated in section C. This approach is *setting-free* and it does not require additional hardware infrastructure or additional engineering costs. Fig. 8 depicts the summary of the proposed solution.

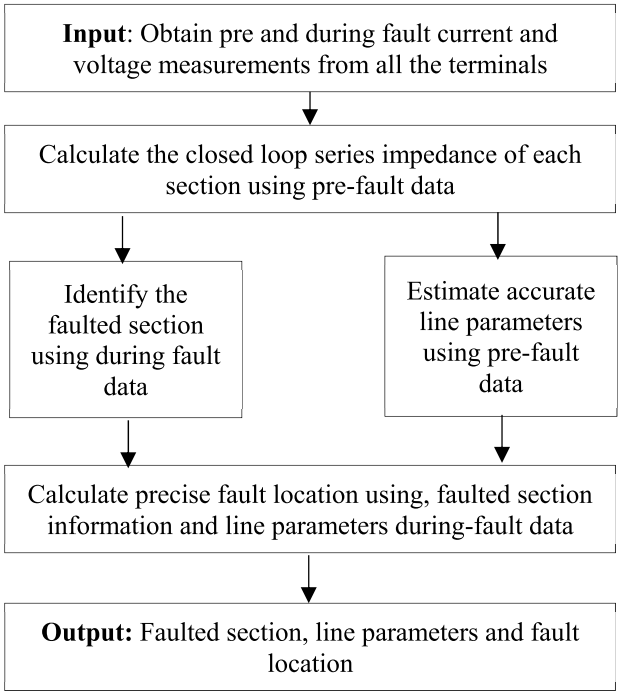

FIGURE 8. Flowchart of the proposed solution.

III. RESULTS AND ANALYSIS

The results for lines connected with conventional/inverter-based renewable resources are presented in this section, along with illustrative examples. A detailed investigation of the developed solution with numerous power system fault situations is also presented. The impact of change in each section's electrical and source parameters on practically existing FL methods along with the proposed solution is also discussed in this section.

A. ILLUSTRATIVE EXAMPLE FOR TTHTL CONNECTED WITH CONVENTIONAL SOURCES AT ALL TERMINALS

A detailed analysis of the developed method has been presented in this section. COMTRADE99 format is used to record the fault data. The algorithm has been verified through MATLAB scripts. The sampling rate used in this method is 1kHz, the phasors are obtained through the DFT technique. The proposed method has been tested for 220kV, 50 Hz

TABLE 1. Determined electrical parameters of each section of TTHTL.

Section	Method	R(mΩ/km)	L(mH/km)
SJ, RJ	Actual	18.79	1.0387
	Proposed	21.28	1.0390
	Error (%)	13.25	0.0289
TJ	Actual	16.28	0.3339
	Proposed	18.36	0.3192
	Error (%)	12.77	4.41

system, with the length of each section being: SJ-80km, RJ-40km, and TJ-20km.

Case 1- *AB fault on SJ section at 40 km from Terminal S with* R_F *10*Ω: The test system considered for this case is derived by closing switch S1 in Fig. 2, all the terminals are connected to conventional sources. Consider the AB fault on the SJ section at 40km from terminal S on the OHL with a fault resistance of 10Ω. The current and voltage signals measured at Bus S, Bus R, and Bus T are shown in Fig. 9(a), (b), and (c) respectively.

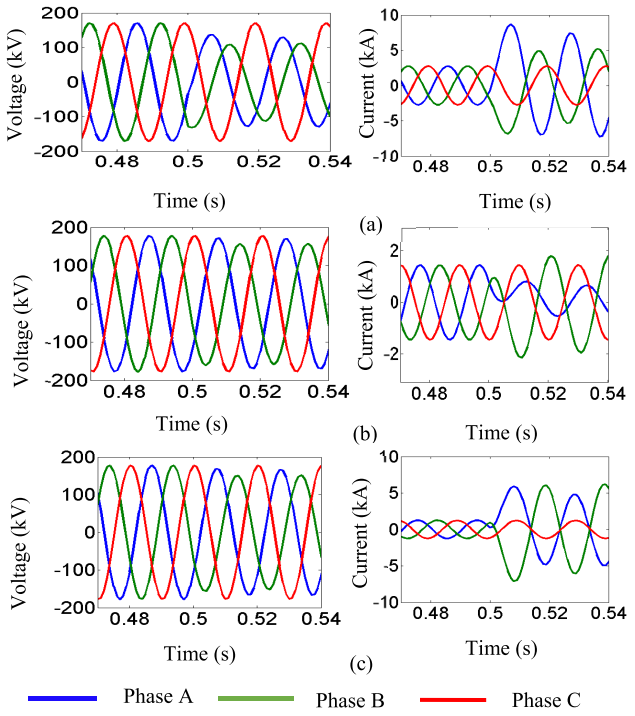

FIGURE 9. Voltages and currents recorded at (a) Bus S, (b) Bus R, and (c) Bus T, for AB fault at 40km from Bus S.

The calculated series impedance in a closed loop form and estimated line parameters are obtained using pre-fault data. For this case, the respective error of each parameter when compared to actual electrical parameters of each section are provided in Tables 1 and 2 respectively. From the tables, it is observed that the series impedance calculated from

TABLE 2. Estimated line parameters using distributed line model.

Section	Method	R(mΩ/km)	L(mH/km)	C(nF/km)
SJ, RJ	Actual	18.79	1.0387	16.18
	Proposed	18.84	1.0387	15.93
	Error (%)	**0.28**	**0.002**	**1.54**
TJ	Actual	16.28	0.3339	25.74
	Proposed	16.39	0.3365	25.90
	Error (%)	**0.71**	**0.07**	**0.652**

TABLE 3. Identified faulted section and fault location.

Actual FS	Identified FS	Actual FL (km)	Calculated FL (km)	FL Error (%)
SJ	SJ	40	40.02	**0.02**

Section II-B and the line parameters estimated from Section II-D are well matched to the actual parameters. The identified faulted section and calculated fault location are presented in Table 3. The faulted section is identified correctly using the calculated series impedance parameters. The estimated parameters are utilized to obtain the FL as they are highly precise than the determined parameters using closed loop formulae. The fault location obtained using the during fault phasors and estimated line parameters is 40.02 km. The obtained FL error using (35) is 0.02%.

$$\%\text{Error} = \left| \frac{\text{Actual Fault Location-Calculated Fault Location}}{\text{Total line length}} \right| \times 100 \tag{35}$$

B. STUDY FOR TTHTL CONNECTED WITH INVERTER-BASED RENEWABLE RESOURCES

This section presents illustrative example cases for the validity of the proposed method with different inverter-based resources such as wind type IV and solar PV plants. The wind and solar modeling details are provided below for this study.

1) MODELING OF INVERTER-BASED RENEWABLE RESOURCES (WIND TYPE IV)

The 200 MW generator consists of 100 units and each unit is of 2 MW rated power. The output of the generator is at 0.69 kV which is stepped up to the collector level voltage of 33kV and then further to the PCC voltage of 220 kV. The Type IV wind turbine generator is a full converter-based generator where the whole power is evacuated to the grid through back-to-back converters (Fig. 10(a)) [49]. Various control strategies to maximize the power delivery of the grid connected IBR have been proposed [50], [51]. The schematic of the control strategy which is achieved in a synchronous reference frame is provided in Fig. 10(b) [52]. The outer

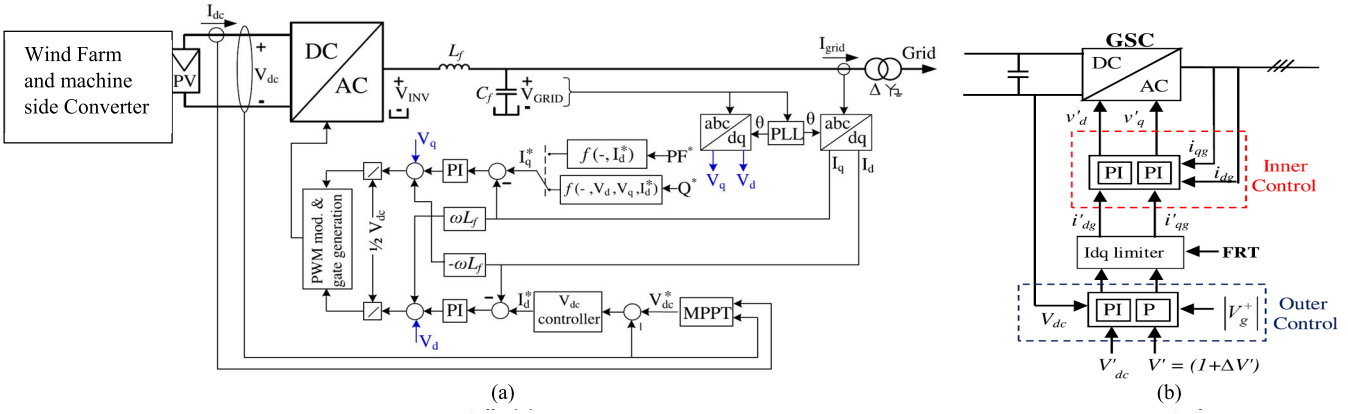

FIGURE 10. Wind Type IV generator modeling details (a) detailed control scheme, and (b) schematic of the grid side inverter control.

TABLE 4. Source Impedances for conventional sources.

Sequence	Terminal S-end	Terminal R-end	Terminal T-end
Positive	3.80 + 30.9i Ω	2.80 + 26.0i Ω	2.50 + 20.0i Ω
Negative	3.80 + 30.9i Ω	2.80 + 26.0i Ω	2.50 + 20.0i Ω
Zero	7.17 + 52.65i Ω	6.2 + 48.546i Ω	5.5 + 45.5i Ω

TABLE 5. Simulation parameters of inverters.

Element	Parameter	Value
Wind generator	Number of units	100
	Rated power of each unit	2 MW
PCC Transformer	Voltage level, frequency	33/220 kV, 50Hz
	MVA rating	500 MVA
	Vector group	YNd11
PI controller	Current control (d,q axis)	$K_p = 1, T_i = 0.02$s
DC bus	Rated voltage	1.45 kV
	DC link capacitor	15000 μF
Filter	L_f, C_f, R_f	335 μH, 200 μF, 0.025 Ω

control loop generates q axis current reference aimed at maintaining PCC voltage magnitude at a reference of 1pu (voltage control). Further, d axis current reference is generated aimed at maintaining the DC link voltage at the reference of 1pu. The current limiter is applied on the q-axis and d-axis current references generated from the outer loop, to limit the total current to the set limit of 1.1pu. Further, the inner control loop generates the converter reference voltages for the grid-side converter. Feedforward compensation to decouple the wind generator from the grid is also included. This ensures balanced voltage across the filter, even during unbalanced conditions at the grid end. In addition to these, the fault ride through (FRT) capability is also implemented which ensures additional reactive current injection during low voltage conditions. A gain (k) of 2 (which determines the rate of reactive current injection in proportion to the dip in PCC voltage) and a dead band of 0.1 is provided (which means the additional injection starts only if the dip in voltage is greater than 0.1pu) (Fig. 11) [49]. However, these FRT requirements depend on the grid code [18]. The parameters of the wind generator are summarized in Table 5.

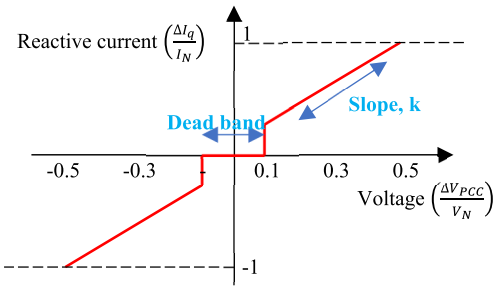

FIGURE 11. Fault ride through (FRT) characteristic.

2) ILLUSTRATIVE CASES—THREE TERMINAL HYBRID LINES CONNECTED WITH RENEWABLE RESOURCES

In this section, we simulated different cases for three-terminal hybrid lines connected with IBRs. The analysis is provided below.

Case 1*- A-g fault on TJ section at 10 km from Bus T with R_F 2 Ω*: The test system considered for this case is derived by closing switch S2 in Fig. 2, terminals S, and R are connected to conventional sources and terminal T is connected to a type IV Wind farm. The current and voltage signals measured at Bus S, Bus R, and Bus T are shown in Fig. 12(a), (b), and (c) respectively. From Fig. 12, the current magnitude is limited and modulated (appears like a balanced fault (see Fig. 12(c)) for IBR connected terminal due to different converter control and grid codes followed by the IBR. Despite such unusual behavior of the IBR-connected terminal current signals, the proposed method provides accurate results. For this case, the calculated series impedance in a closed loop form, estimated electrical parameters of each section of TTHTL, and their errors with respect to the actual electrical parameters of each section are provided in Tables 6 and 7 respectively.

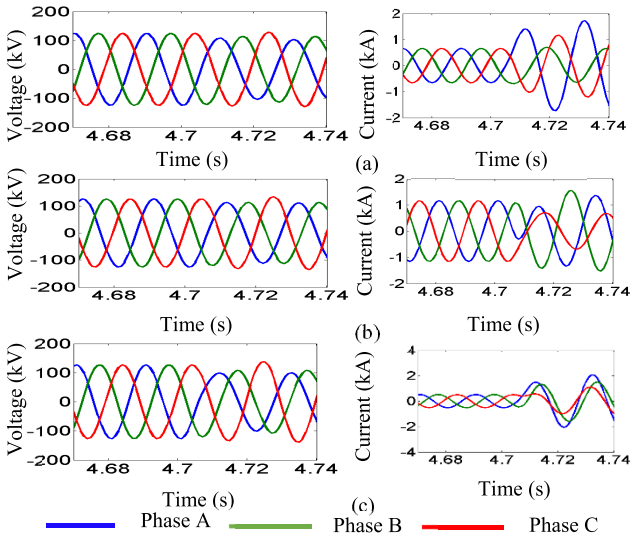

FIGURE 12. Voltages and currents measured at (a) Bus S, (b) Bus R and (c) Bus T, for A-g fault at 10km from Bus T.

The identified faulted section and calculated fault location are presented in Table 8. The calculated series impedance identifies the faulted section accurately. Precise FL is obtained using the estimated electrical parameters of each section of TTHTL for this case. Integration of the wind farm at Bus T did not affect the proposed method and provided accurate results. The error in fault location obtained for this case is 0.02% which is within two tower span distance.

Case 2- *BC-g fault on RJ section at 110 km from Bus S with* R_F *20* Ω: The test system considered for this case is derived by closing switch S3 in Fig. 2, terminals S, and R are connected to conventional sources and terminal T is connected to the solar power plant. The solar park is modeled as a full converter model [53]. The current and voltage signals measured at Bus S, Bus R, and Bus T are shown in Fig. 13(a), (b), and (c) respectively. For this case, the determined series impedance in a closed loop form, estimated electrical parameters of each section of TTHTL, and their errors with respect to the actual section parameters are presented in Tables 9 and 10 respectively. The identified faulted section and calculated fault location are presented in Table 11. The table shows the calculated/estimated electrical parameters of each section accurately even for the solar park connected at terminal T. The faulted section and location are achieved correctly for these cases using the estimated parameters. The error in fault location obtained for this case is 0.48%. The integration of renewable sources like solar PV, has the least impact on the proposed method as it uses all side measurements [20]. The non-homogeneity introduced by IBRs are compensated [43] by using all side measurements.

Case 3- *A-g fault at Junction with* R_F *50* Ω: The test system considered for this case is derived by closing switch S2 and S3 in Fig. 2, terminals S, and R are connected to conventional sources and terminal T is connected to a type IV Wind farm and Solar PV. The current and voltage signals

TABLE 6. Determined electrical parameters of each section of TTHTL.

Section	Method	R(mΩ/km)	L(mH/km)
SJ, RJ	Actual	18.79	1.0387
	Proposed	21.81	1.0398
	Error (%)	16.07	0.11
TJ	Actual	16.28	0.3339
	Proposed	18.48	0.3194
	Error (%)	13.51	4.34

TABLE 7. Estimated line parameters using distributed line model.

Section	Method	R(mΩ/km)	L(mH/km)	C(nF/km)
SJ, RJ	Actual	18.79	1.0387	16.91
	Proposed	18.73	1.0387	15.93
	Error (%)	**0.32**	**0.002**	**4.46**
TJ	Actual	16.28	0.3339	25.74
	Proposed	17.11	0.3364	25.28
	Error (%)	**5.04**	**0.76**	**1.75**

TABLE 8. Identified faulted section and fault location.

Actual FS	Identified FS	Actual FL (km)	Calculated FL (km)	FL Error (%)
TJ	TJ	10	10.03	**0.025**

TABLE 9. Determined electrical parameters of each section of TTHTL.

Section	Method	R(mΩ/km)	L(mH/km)
SJ, RJ	Actual	18.79	1.0387
	Proposed	21.81	1.039
	Error (%)	16.05	0.08
TJ	Actual	16.28	0.3339
	Proposed	19.11	0.3178
	Error (%)	17.35	4.82

measured at Bus S, Bus R, and Bus T are shown in Fig. 14(a), (b), and (c) respectively. From Fig. 14, reduced the currents at terminal R and another terminal are increased. The current signal is modulated at terminal T due to inverter controls. The junction faults are very common for the three-terminal hybrid lines. For this case, the calculated series impedance in a closed loop form, estimated electrical parameters of each section, and their deviations with respect to the actual parameters of each section are presented in Tables 12 and 13. From the table, OHL section parameters errors are within 1%. The identified faulted section and calculated fault location

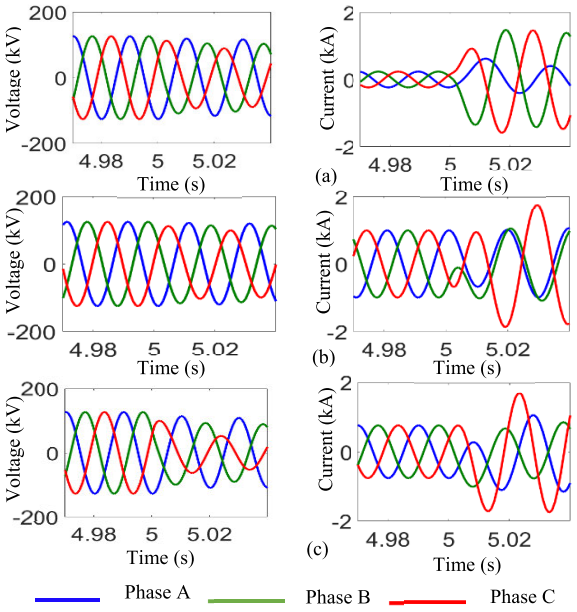

FIGURE 13. Voltages and currents measured at (a) Bus S, (b) Bus R and (c) Bus T, for BC-g fault at 110km from Bus S.

TABLE 10. Estimated line parameters using distributed line model.

Section	Method	R(mΩ/km)	L(mH/km)	C(nF/km)
SJ, RJ	Actual	18.79	1.0387	16.91
	Proposed	18.82	1.0386	16.37
	Error (%)	**0.16**	**0.012**	**1.19**
TJ	Actual	16.28	0.3339	25.74
	Proposed	16.73	0.336	25.62
	Error (%)	**2.74**	**0.62**	**0.44**

TABLE 11. Identified faulted section and fault location.

Actual FS	Identified FS	Actual FL (km)	Calculated FL (km)	FL Error (%)
RJ	RJ	110	109.98	**0.02**

are presented in Table 14. The faulted section is identified as a junction fault for this case as all calculated and measured voltage differences are less than the threshold.

The fault location provided for this case is section lengths from each terminal. For example, IED at terminal S provides the fault location is 80km.

***Case 4**-BC-g fault on RJ section at 105 km from Bus S with R_F 20 Ω* : The test system considered for this case is shown in Fig. 15, terminal S is connected to a conventional source, R is connected to the solar power plant and T is connected to a type IV Wind farm. This arrangement might not be feasible today, however, this could be a possible scenario for future renewable integration systems. The current and voltage

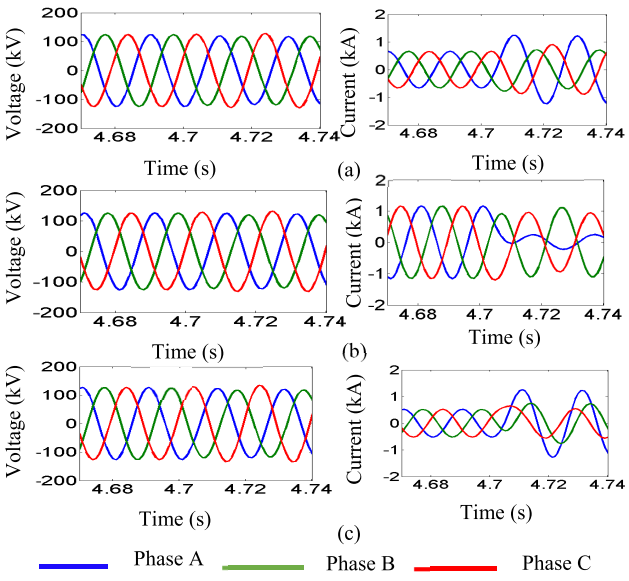

FIGURE 14. Voltage and current signals measured at (a) Bus S, (b) Bus R and (c) Bus T for A-g fault at junction.

TABLE 12. Determined electrical parameters of each section of TTHTL.

Section	Method	R(mΩ/km)	L(mH/km)
SJ, RJ	Actual	18.79	1.0387
	Proposed	22.05	1.0382
	Error (%)	17.35	0.044
TJ	Actual	16.28	0.3339
	Proposed	19.965	0.317
	Error (%)	22.64	4.96

TABLE 13. Estimated line parameters using distributed line model.

Section	Method	R(mΩ/km)	L(mH/km)	C(nF/km)
SJ, RJ	Actual	18.79	1.0387	16.91
	Proposed	18.85	1.0387	16.24
	Error (%)	**0.34**	**0.004**	**0.41**
TJ	Actual	16.28	0.3339	25.74
	Proposed	16.78	0.334	25.69
	Error (%)	**3.11**	**0.08**	**0.14**

TABLE 14. Identified faulted section and fault location.

Actual FS	Identified FS	Actual FL (km)	Calculated FL (km)	FL Error (%)
Junction	Junction	80	80	0.0

signals measured at Bus S, Bus R, and Bus T are shown in Fig. 16(a), (b), and (c) respectively.

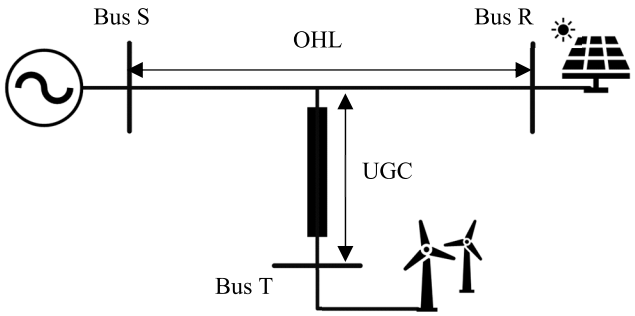

FIGURE 15. Three-terminal hybrid line connected to conventional, wind farm and solar plants.

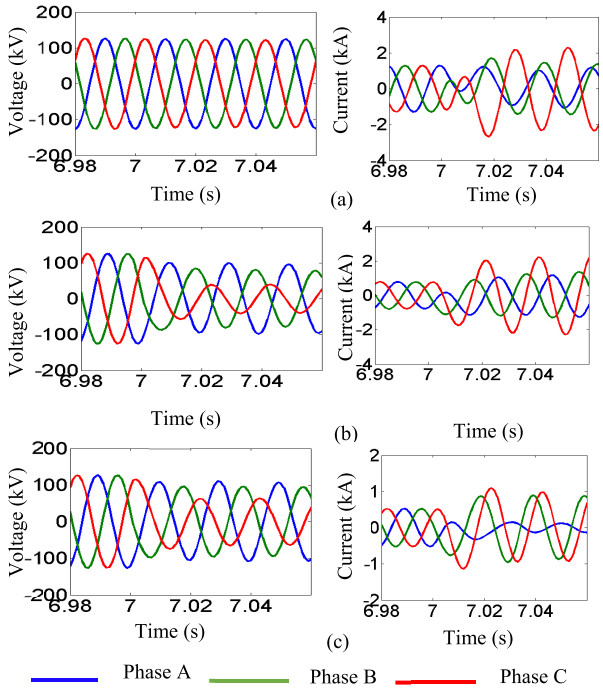

FIGURE 16. Pre and fault voltages and currents measured at (a) Bus S, (b) Bus R and (c) Bus T for BC-g fault at 105km from Bus S.

For this case, the calculated series impedance in a closed loop form, estimated line parameters, and their corresponding errors with respect to the actual line parameters are provided in Tables 15 and 16 respectively. The identified faulted section and calculated fault location are presented in Table 17. From table 16, the estimated parameter is accurate and the error in inductance estimation is less than 1%. The faulted section is accurately identified as "RJ" and the location is calculated as 105.08km. The fault location error is less than 0.1%. The proposed solution is not affected even by two terminals connected with IBRs. The proposed solution is suitable for future power system scenarios.

C. COMPREHENSIVE STUDY USING DIFFERENT TEST SYSTEMS AND CONDITIONS

The proposed solution is tested for various combinations of the IBRs with various power system fault conditions. The test cases are presented in Table 18. A total of **4320** fault cases are tested; the average and maximum errors of parameters of each section are provided in Table 19. From the table, the average error is less than 2% which is suitable for fault

TABLE 15. Determined electrical parameters of each section of TTHTL.

Section	Method	R(mΩ/km)	L(mH/km)
SJ, RJ	Actual	18.79	1.0387
	Proposed	15.15	1.042
	Error (%)	19.37	0.32
TJ	Actual	16.28	0.3339
	Proposed	19.95	0.315
	Error (%)	22.54	5.66

TABLE 16. Estimated line parameters using distributed line model.

Section	Method	R(mΩ/km)	L(mH/km)	C(nF/km)
SJ, RJ	Actual	18.79	1.0387	16.91
	Proposed	18.74	1.0387	16.03
	Error (%)	**0.23**	**0.003**	**1.04**
TJ	Actual	16.28	0.3339	25.74
	Proposed	15.67	0.334	25.83
	Error (%)	**3.73**	**0.07**	**0.36**

TABLE 17. Identified faulted section and fault location.

Actual FS	Identified FS	Actual FL	Calculated FL	FL Error (%)
RJ	RJ	105	105.08	**0.07**

TABLE 18. Various fault conditions and test system configurations.

Test Cases		Test Conditions
Fault location (km)	From terminal S	10, 20, 40, 70, 85, 90, 110
	From terminal T	5, 10, 15
Fault type		A-g, AB, BC-g, and ABC-g
Fault Inception Angle		0^0 and 90^0
Fault resistance (Ω)		0.1, 2, 5, 10, and 50
SIR (S: R: T)		0.5:1:2, and 1:2:0.5
Load		50%, 100 % and 125%
Test system configuration		1. All conventional resources 2. Connected with two conventional and Wind Type IV at Terminal T 3. Connected with one conventional and Wind Type IV at Terminal T and Solar PV at Terminal R

TABLE 19. Average and maximum error of estimated line parameters.

Parameter	R(mΩ/km)		L(mH/km)		C(nF/km)	
Section /Error (%)	Avg.	Max.	Avg.	Max.	Avg.	Max.
SJ, RJ	1.85	9.06	0.16	1.01	1.99	10.18
TJ	2.04	14.12	0.74	3.32	1.49	6.45

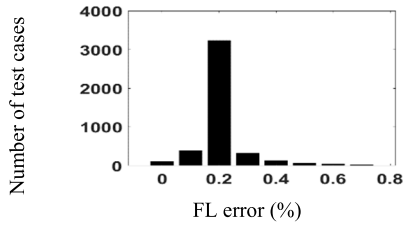

FIGURE 17. Performance summary of the developed FL solution for various fault situations.

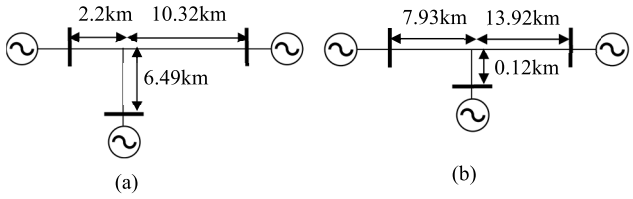

FIGURE 18. Practical three-terminal systems (a) Test System 1 and (b) Test System 2.

location and protection setting calculations. The faulted section is identified correctly for all the cases and the fault location error is demonstrated in Fig. 17. From Fig. 17, the maximum fault location error is 0.68%. The average fault location error is 0.2% (∼240m) for about 3450 (∼80%) cases which is within two tower span (300m) distance. The fault location is not influenced by the fault type, fault resistance, loading of the line, SIRs (line to source impedance ratio), and location of the inverter-based renewable resource.

D. PERFORMANCE EVALUATION FOR PRACTICAL INDIAN SYSTEMS

The proposed method is tested with two practical systems as shown in Fig. 18. These lines are connected to a 110kV, 50Hz supply. A total of 144 cases are tested for each test system covering different fault types, fault resistance, fault inception angles, and locations of the fault. The parameter estimation algorithms are accurately working for these test systems even for a short line with taps. The average and maximum errors in parameter estimation are provided in Tables 20 and 21. From the tables, the proposed method calculated the parameters accurately for Test Systems 1 and 2. The faulted section identified for Test Systems 1 and 2 and fault locations for the cases are provided in Table 22. The faulted section is identified accurately for both test systems. Two cases failed for Test System 2 as the fault is very close to the junction on

TABLE 20. Average and maximum error of estimated line parameters of test system 1.

Parameter	R(mΩ/km)		L(mH/km)		C(nF/km)	
Section / Error (%)	Avg.	Max.	Avg.	Max.	Avg.	Max.
SJ, RJ	1.15	4.12	0.11	0.97	0.92	2.18
TJ	1.14	3.12	0.14	1.32	0.79	2.45

TABLE 21. Average and maximum error of estimated line parameters of test system 2.

Parameter	R(mΩ/km)		L(mH/km)		C(nF/km)	
Section / Error (%)	Avg.	Max.	Avg.	Max.	Avg.	Max.
SJ, RJ	1.25	3.86	0.12	1.02	0.91	2.2
TJ	1.24	14.12	0.13	1.12	0.82	2.22

TABLE 22. Reliability of FSI and FL error (%) for test system 1 and 2.

Test System	FSI Reliability (%)	Fault Location Error in (meters)	
		Average FL Error (m)	Maximum FL Error (m)
1	100	220	325
2	99	305	524

section SJ. This fault is identified as a Junction fault as section SJ is very short (0.12km). The average fault location error for both the test systems is close to 300m (i.e., close to two tower span distance) which is the best accuracy as per the industry standards for these complex systems.

E. COMPARATIVE ANALYSIS WITH COMMERCIALLY AVAILABLE METHODS FOR TTHTLs

This section compares the performance of the proposed solution with practically proven positive [38] and negative [33] sequence-based methods. These methods require the line parameters as input. The accuracy of fault location highly depends on the parameters of each section such as resistance, inductance, and capacitance. These parameters are never accurate most of the time, as these parameters change with temperature, aging, the sag of the conductor, etc., of the line, especially in cable sections. A comparison of the proposed method with commercially established positive sequence (PSFL) [38] and negative sequence (NSFL) [33] methods for lines connected with conventional and IBRs is presented in this section.

1) THREE TERMINAL HYBRID LINES CONNECTED WITH CONVENTIONAL SOURCES

This section provides the comparative assessment of the line and source impedance parameter variation on the proposed method (PM), positive sequence (PSFL) [38], and negative

sequence (NSFL) [33] for lines connected with conventional sources.

a: VARIATION IN EACH SECTION PARAMETERS

Consider a phase-to-ground (A-g) fault at 50km from terminal SJ. The fault resistances considered for the fault are 20 Ω and the FIA is 0^0. By varying the line parameters (resistance, inductance, capacitance) with error of 0% to 50%, the fault location errors for the proposed method (PM) and practical methods are evaluated. The evaluation result for the fault case is shown in Fig. 19. From the figure, it is observed that the fault location errors of PSFL [38] and NSFL [33] increases with the increase in the error in section parameters whereas the FL error for PM is not impacted by the parameter variation in this case. For a 10% variation in the line parameters, the FL error for practical methods is more than 3%. This requires a significant amount of time, and more towers need to be inspected for the existing methods. The accuracy of the main and tapped lines parameters has a significant impact on the FL accuracy claimed by existing methods.

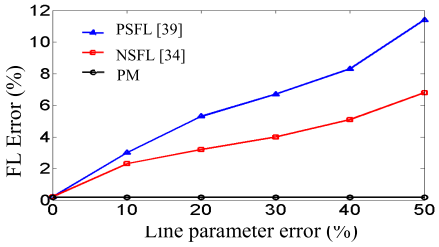

FIGURE 19. Comparative analysis of the developed solution vs commercially established solutions for change in the parameters of TTHTLs for A-g fault at 50km from Terminal S.

b: VARIATION IN SOURCE PARAMETERS

The presented solution using negative sequence quantities [33] requires equivalents of sources magnitudes parameters as a setting. The magnitudes of the source equivalent change with changes in operational and structural conditions in the interconnected power system. A comparative assessment of the developed and practically available FL solution for source impedance magnitude changes, is presented in this section. For this case, we have considered a phase-to-ground (A-g) fault on tapped line (i.e., 15km from Terminal T). The fault resistance for A-g fault is 1Ω as practical fault resistance on cable is very small due to the small arc length in between the core and sheath.

By varying the error in magnitude of source impedance from 0% to 50%, the performance of the proposed method is validated. The results of the analysis for these cases are shown in Fig. 20. From the figure, PSFL [38], and proposed method fault location accuracies are not impacted by the source parameter variation for this case, but the fault location error of negative sequence [33] increases with increase in error of source impedance magnitudes parameters. The negative sequence-based method [33] is greatly affected by the variation in source impedance magnitude. With the integration of renewables into the grid, the source strength varies enormously, and the accuracy of the method [33] will only get worse for networks with integrated renewable sources.

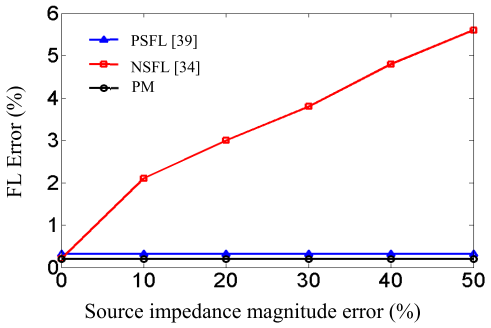

FIGURE 20. Comparative assessment of the developed vs commercially established solutions for change in the source equivalent magnitude for A-g fault at 15km from Terminal T.

2) THREE TERMINAL HYBRID LINES CONNECTED WITH INVERTER-BASED RENEWABLE SOURCES

This section provides the comparative assessment of the line and source impedance parameter variation on the proposed method (PM), positive sequence (PSFL) [38], and negative sequence (NSFL) [33] for lines connected with inverter-based renewable resources.

a: INVERTER-BASED RESOURCES CONNECTED AT TAPPED LINE TERMINAL T

The test system considered for this case is derived by closing switch S2 in Fig. 2, terminals S, and R are connected to conventional sources and terminal T is connected to wind type IV. With the integration of renewable power plant in the present scenario, this configuration is very common. Let us examine how effectively the existing and proposed method behaves for this configuration. Consider an A-g fault on the transmission line at 75 km from terminal S having a fault resistance of 10 Ω, with a fault inception angle of 0°.The faulted section is correctly identified by the proposed and positive sequence-based method [38]. However, the positive sequence-based method [38] requires each section parameter as an input. The calculated fault distances using PSFL [38] and the proposed method are 75.8 km and 74.72 km respectively. The absolute percentage of fault location errors of PSFL and PM are 0.6% and 0.2% respectively for this case. The proposed and positive sequence methods are not affected by renewable integration. However, the performance of PSFL [38] highly depends on the precision of the parameters of the line.

The solution presented using negative sequence quantities [33] is not worked for this method as the negative sequence current is not available at Terminal T as shown in Fig. 21. NSFL [33] will not provide reliable results for lines connected with inverter-based renewable resources (Solar PV or Wind type IV) as most of the grid codes will not provide the negative sequence currents [18], [19]. Moreover, the source

TABLE 23. A comparative analysis with existing approaches.

Method	Required Inputs	Factors affecting the accuracy of fault location for existing and proposed methods			
		Fault Type	Initial Guess	Line Parameters	Renewable Integration
[33]	Negative sequence voltage and current signals from all terminals	Yes	No	Yes	Yes
[34]	Positive and negative sequence voltage and current signals from two terminals	Yes	Yes	Yes	Yes
[38]	Positive sequence voltage and current signals from all terminals	No	No	Yes	No
[47]	Positive sequence voltage and current signals from all terminals	No	Yes	No	No
PM	Positive sequence voltage and current signals from all terminals	No	No	No	No

impedance of the inverter-based resource is continuously varying during the fault period and the method [33] is not reliable for renewable connected systems.

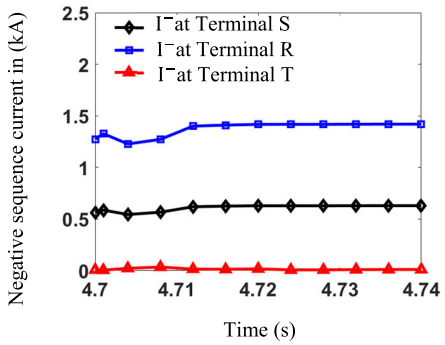

FIGURE 21. Shows recorded negative sequence quantities at all terminals for A-g fault at 75km from terminal S.

b: INVERTER-BASED RESOURCES CONNECTED AT MAIN LINE AT TERMINAL R AND TAPPED LINE TERMINAL T

The test system considered for this case is shown in Fig. 15. The Type IV wind farm is connected at tapped line Terminal T and solar PV is connected at Terminal R. This type of configuration may not be common today, but it may be possible in future renewable connected systems. Let us examine how effectively the existing and proposed method behaves for this configuration. Consider AB fault on the hybrid line at 5km from Terminal T having a fault resistance of 2Ω with a fault inception angle of 0°. The faulted section is correctly identified by proposed and positive sequence [38] methods. The estimated fault distances using PSFL [38] and the proposed method are 5.4km and 4.68km respectively. The absolute percentage of fault location errors of PSFL and PM are 0.33% and 0.26% respectively for this case. The proposed and positive sequence methods are not affected by renewables connected with two ends of three- NSFL [33] failed to calculate the faulted section and fault location for the lines connected with renewable resources. The negative

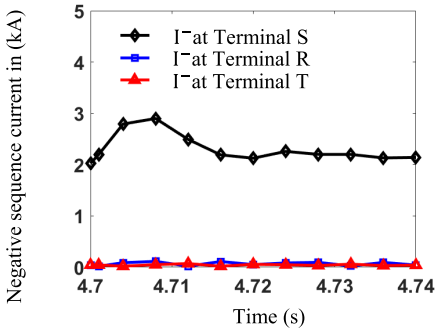

FIGURE 22. Shows negative sequence current measured at all terminals for AB fault at 5km from terminal T.

sequence-based method [33] does not work as the negative sequence currents are not available at terminals T and R as shown in Fig. 22.

F. QUALITATIVE ANALYSIS OF RECENT LITERATURE

The proposed method is compared with the practically proven methods [33], [38] and found to be superior with various fault types, fault resistance, source impedances, and different network configurations. Further, the proposed method is compared with recent methods [34], [47]. The method in [34] computes fault location using the two-ends data of a three-terminal line, the third terminal being connected to renewable energy sources (RES) using positive and negative sequence quantities. Method [34] requires negative sequence quantities which are not available for balanced faults, and it requires line parameters as input. These line parameters are varying due to changes in temperature, aging, the sag of the conductor, etc., of the line and this would affect the accuracy of the fault location. The method in [47] uses positive sequence quantities to obtain the fault location along with the line parameters using the trust region optimization algorithm. Implementation of such a high computational method in the IED platform is difficult. The success of the method depends on the proper initial guess. The proposed method overcomes limitations

of [34] and [47], as it computes initial guess in a closed-loop form which makes it computationally less intensive. It is also advantageous in comparison to the method in [34], as it does not require line parameters as settings and works for all fault types. A detailed comparison is provided in Table 23 by taking into consideration the factors that affect the accuracy of fault location. This will help to choose the appropriate fault locator for practical usage by utility providers.

IV. CONCLUSION

In this work, a setting-free fault section identification and fault location estimation solution using all terminal voltages and currents for a TTHTL connected with conventional or IBRs is presented. The main advantages of the proposed method are summarized as follows.

- The proposed method eliminates the requirement of line parameters of each section as settings, which enhances the accuracy of the solution and reduces engineering cost and time.
- One of the main contributions of the proposed method is that the fault section is identified using closed-loop formulae which can be used for selective/adaptive auto-reclosing protection schemes for hybrid lines.
- The performance of the proposed solution correctly identifies the faulted section and locates the fault accurately for TTHTLs connected with conventional/inverter-based renewable resources for various fault situations including various grid codes.
- The proposed method is compared with the commercially existing methods and found to be superior with various fault types, fault resistance, source impedances, and different network configurations.
- The proposed method is tested with two practical Indian systems and the method works well for these systems.
- Obtained results show that, with various fault scenarios, the fault section identification achieved 100% reliability, and the average FL precision is around 0.2%. It is predictable that the accuracy of the FL will be within 2 tower spans for TTHTLs connected with conventional/IBRs.
- Another interesting attribute of the proposed method is that it does not need additional infrastructure other than what is needed for a line differential protection scheme, i.e., a 2 Mbps communication link, and no additional hardware cost is incurred.
- The proposed method is suitable to calculate the reliable faulted section and determine the distance to fault accurately in rugged transmission terrains (for example, coastal, high/low temperature countries, deserts, etc.) as it does not dependent on the cable parameters and the parameters of each section, which vary with change in temperatures.
- Moreover, the determined electrical parameters of each section can be used for power system monitoring and protection application settings.

In future work, the developed solution can be implemented in cloud-based platforms or SCADA/EMS control centers. The issues with measurement errors and data synchronization can be eliminated in future works.

REFERENCES

[1] *Protection Aspects of Multi-Terminal Lines*, IEEE Power System Relaying Committee (PSRC), New York, NY, USA, 1980.
[2] *Protection Aspects of Multi Terminal Lines*, document TH0056-2-PWR, IEEE Power System Relaying Committee, 1979.
[3] D. A. Tziouvaras and J. Needs, "Protection of mixed overhead and underground cable lines," in *Proc. 12th IET Int. Conf. Develop. Power Syst. Protection (DPSP)*, 2014, pp. 1–6.
[4] S. Sarangi and A. K. Pradhan, "Adaptive direct underreaching transfer trip protection scheme for the three-terminal line," *IEEE Trans. Power Del.*, vol. 30, no. 6, pp. 2383–2391, Dec. 2015.
[5] R. K. Aggarwal and A. T. Johns, "The development of a new high speed 3-terminal line protection scheme," *IEEE Power Eng. Rev.*, vol. PER-6, no. 1, p. 43, Jan. 1986.
[6] N. Jin, X. Lin, J. Xing, Z. Li, S. Liu, L. Chen, X. Ma, Z. Rong, and N. Tong, "Research on multiterminal current differential protection criterion with high sensitivity and synchronization error tolerance capability," *IEEE Trans. Power Del.*, vol. 33, no. 6, pp. 3085–3094, Dec. 2018.
[7] Hitachi Energy Product Guide. *Line Differential Protection RED6702.1*. Accessed: Mar. 2019. [Online]. Available: https://search.abb.com/library/Download.aspx?DocumentID=1MRK505346-BEN&LanguageCode=en&DocumentPartId=&Action=Launch
[8] *IEEE Guide for Automatic Reclosing of Circuit Breakers for AC Distribution and Transmission Lines*, IEEE Standard C37.104-2012, Jul. 2012, doi: 10.1109/IEEESTD.2012.6232415.
[9] *Short Circuit Protection of Circuits With Mixed Conductor Technologies in Transmission Networks*, CIGRE, Paris, France, Jun. 2014.
[10] N. George and O. D. Naidu, "Traveling wave based autoreclosure scheme for multi-terminal lines," in *Proc. IEEE PES Innov. Smart Grid Technol. Conf. Eur.*, Sep. 2017, pp. 1–6.
[11] O. D. Naidu, A. K. Pradhan, and P. Krishnamurthy, "Traveling wave based adaptive auto-reclosing and fault location for three-terminal mixed lines," in *Proc. IEEE PES GTD Grand Int. Conf. Expo. Asia*, Mar. 2019, pp. 466–471.
[12] R. J. Hamidi and H. Livani, "Traveling-wave-based fault-location algorithm for hybrid multiterminal circuits," *IEEE Trans. Power Del.*, vol. 32, no. 1, pp. 135–144, Feb. 2017.
[13] H. Livani and C. Y. Evrenosoglu, "A machine learning and wavelet-based fault location method for hybrid transmission lines," *IEEE Trans. Smart Grid*, vol. 5, no. 1, pp. 51–59, Jan. 2014.
[14] A. Tabatabaei, M. R. Mosavi, and P. Farajiparvar, "A traveling-wave fault location technique for three-terminal lines based on wavelet analysis and recurrent neural network using GPS timing," in *Proc. Smart Grid Conf. (SGC)*, Dec. 2013, pp. 268–272.
[15] S. Zhang, H. Gao, and Y. Song, "A new fault-location algorithm for extra-high-voltage mixed lines based on phase characteristics of the hyperbolic tangent function," *IEEE Trans. Power Del.*, vol. 31, no. 3, pp. 1203–1212, Jun. 2016.
[16] O. Naidu, P. Yalla, and N. George, "Auto-reclosing protection scheme for multi-terminal mixed lines using synchrophasor measurements," in *Proc. Int. Conf. Smart Grid Synchronized Meas. Anal. (SGSMA)*, May 2019, pp. 1–6.
[17] O. D. Naidu, N. George, and P. Yalla, "Setting-free fault section identification and fault location method for three-terminal lines," in *Proc. 9th Int. Conf. Power Energy Syst. (ICPES)*, Dec. 2019, pp. 1–6.
[18] A. Hooshyar, M. A. Azzouz, and E. F. El-Saadany, "Distance protection of lines emanating from full-scale converter-interfaced renewable energy power plants—Part I: Problem statement," *IEEE Trans. Power Del.*, vol. 30, no. 4, pp. 1770–1780, Aug. 2015.
[19] S. Paladhi and A. K. Pradhan, "Adaptive distance protection for lines connecting converter-interfaced renewable plants," *IEEE J. Emerg. Sel. Topics Power Electron.*, vol. 9, no. 6, pp. 7088–7098, Dec. 2021.
[20] N. George and O. D. Naidu, "Distance protection issues with renewable power generators and possible solutions," in *Proc. 16th Int. Conf. Develop. Power Syst. Protection*, 2022, pp. 1–6.
[21] *IEEE Guide for Determining Fault Location on AC Transmission and Distribution Lines*, IEEE Standard C37.114-2014, Jan. 2015.

[22] M. M. Saha, J. Izykowski, and E. Rosolowski, *Fault Location on Power Networks* (Power Systems). London, U.K.: Springer, 2010.
[23] E. O. Schweitzer, A. Guzman, M. V. Mynam, V. Skendzic, B. Kasztenny, and S. Marx, "Locating faults by the traveling waves they launch," in *Proc. 67th Annu. Conf. Protective Relay Eng.*, Mar. 2014, pp. 95–110.
[24] H. Shu, X. Liu, and X. Tian, "Single-ended fault location for hybrid feeders based on characteristic distribution of traveling wave along a line," *IEEE Trans. Power Del.*, vol. 36, no. 1, pp. 339–350, Feb. 2021.
[25] O. Naidu and A. K. Pradhan, "A traveling wave-based fault location method using unsynchronized current measurements," *IEEE Trans. Power Del.*, vol. 34, no. 2, pp. 505–513, Apr. 2019.
[26] T. Takagi, Y. Yamakoshi, M. Yamaura, R. Kondow, and T. Matsushima, "Development of a new type fault locator using the one-terminal voltage and current data," *IEEE Power Eng. Rev.*, vol. PER-2, no. 8, pp. 59–60, Aug. 1982.
[27] L. Eriksson, M. M. Saha, and G. D. Rockefeller, "An accurate fault locator with compensation for apparent reactance in the fault resistance resulting from remore-end infeed," *IEEE Trans. Power App. Syst.*, vol. PAS-104, no. 2, pp. 423–436, Feb. 1985.
[28] S. Das, S. Santoso, A. Gaikwad, and M. Patel, "Impedance-based fault location in transmission networks: Theory and application," *IEEE Access*, vol. 2, pp. 537–557, 2014.
[29] H. Panahi, R. Zamani, M. Sanaye-Pasand, and H. Mehrjerdi, "Advances in transmission network fault location in modern power systems: Review, outlook and future works," *IEEE Access*, vol. 9, pp. 158599–158615, 2021.
[30] C. Y. Evrenosoglu and A. Abur, "Travelling wave based fault location for teed circuits," *IEEE Trans. Power Del.*, vol. 20, no. 2, pp. 1115–1121, Apr. 2005.
[31] S. Sawai, A. K. Pradhan, and O. D. Naidu, "Traveling wave based fault location of multi-terminal transmission lines," in *Proc. IEEE PES Asia–Pacific Power Energy Eng. Conf. (APPEEC)*, Nov. 2017, pp. 1–6.
[32] A. Ghorbani and H. Mehrjerdi, "Negative-sequence network based fault location scheme for double-circuit multi-terminal transmission lines," *IEEE Trans. Power Del.*, vol. 34, no. 3, pp. 1109–1117, Jun. 2019.
[33] D. A. Tziouvaras, "New multi-ended fault location design for two- or three-terminal lines," in *Proc. 7th Int. Conf. Develop. Power Syst. Protection (DPSP)*, 2001, pp. 395–398.
[34] H. Panahi, M. Sanaye-Pasand, and M. Davarpanah, "Three-terminal lines fault location using two main terminals data in the presence of renewable energy sources," *IEEE Trans. Smart Grid*, early access, Oct. 25, 2022, doi: 10.1109/TSG.2022.3216908.
[35] Y.-H. Lin, C.-W. Liu, and C.-S. Yu, "A new fault locator for three-terminal transmission lines using two-terminal synchronized voltage and current phasors," *IEEE Trans. Power Del.*, vol. 17, no. 2, pp. 452–459, Apr. 2002.
[36] J. Izykowski, E. Rosolowski, M. M. Saha, M. Fulczyk, and P. Balcerek, "A fault-location method for application with current differential relays of three-terminal lines," *IEEE Trans. Power Del.*, vol. 22, no. 4, pp. 2099–2107, Oct. 2007.
[37] N. George, O. Naidu, S. Srivastava, and A. V. S. S. R. Sai, "Fault location for multi-terminal tapped lines using synchronized measurements," in *Proc. IEEE Recent Adv. Intell. Comput. Syst. (RAICS)*, Dec. 2018, pp. 153–158.
[38] T.-C. Lin, J.-Z. Yang, C.-S. Yu, and C.-W. Liu, "Development of a transmission network fault location platform based on cloud computing and synchrophasors," *IEEE Trans. Power Del.*, vol. 35, no. 1, pp. 84–94, Feb. 2020.
[39] V. K. Gaur, B. R. Bhalja, and M. Kezunovic, "Novel fault distance estimation method for three-terminal transmission line," *IEEE Trans. Power Del.*, vol. 36, no. 1, pp. 406–417, Feb. 2021.
[40] Y. Liu, B. Wang, X. Zheng, D. Lu, M. Fu, and N. Tai, "Fault location algorithm for non-homogeneous transmission lines considering line asymmetry," *IEEE Trans. Power Del.*, vol. 35, no. 5, pp. 2425–2437, Oct. 2020.
[41] G. L. Kusic and D. L. Garrison, "Measurement of transmission line parameters from SCADA data," in *Proc. IEEE PES Power Syst. Conf. Expo.*, New York, NY, USA, 2004, pp. 440–445.
[42] M. Asprou and E. Kyriakides, "Identification and estimation of erroneous transmission line parameters using PMU measurements," *IEEE Trans. Power Del.*, vol. 32, no. 6, pp. 2510–2519, Dec. 2017.
[43] O. D. Naidu, S. Zubic, A. V. S. S. R. Sai, A. N. Praveen, P. Cost, and H. Eriksson, "Economical setting-free double-ended fault locator for transmission lines: Experiences from recent pilot installations," *IEEE Access*, vol. 10, pp. 96805–96820, 2022.
[44] L. Zhang and A. Abur, "Identifying parameter errors via multiple measurement scans," *IEEE Trans. Power Syst.*, vol. 28, no. 4, pp. 3916–3923, Nov. 2013.
[45] Y. Liao and M. Kezunovic, "Online optimal transmission line parameter estimation for relaying applications," *IEEE Trans. Power Del.*, vol. 24, no. 1, pp. 96–102, Jan. 2009.
[46] S. S. Mousavi-Seyedi, F. Aminifar, and S. Afsharnia, "Parameter estimation of multiterminal transmission lines using joint PMU and SCADA data," *IEEE Trans. Power Del.*, vol. 30, no. 3, pp. 1077–1085, Jun. 2015.
[47] Z. Yun, T. Wen, and C. Wang, "Fault location method for three-terminal lines in distribution network based on line voltage measured by μMPMU," *IEEE Trans. Smart Grid*, vol. 12, no. 6, pp. 5095–5112, Nov. 2021.
[48] O. D. Naidu, N. George, and P. Yalla, "Parameter estimation, selective auto-reclosing and fault location for three-terminal mixed transmission lines using synchronised data," *IET Gener., Transmiss. Distrib.*, vol. 14, no. 25, pp. 6049–6060, Dec. 2020.
[49] A. Chowdhury, S. Paladhi, and A. K. Pradhan, "Adaptive unit protection for lines connecting large solar plants using incremental current ratio," *IEEE Syst. J.*, vol. 16, no. 2, pp. 3272–3283, Jun. 2022.
[50] D. Çelik and M. E. Meral, "Current control based power management strategy for distributed power generation system," *Control Eng. Pract.*, vol. 82, pp. 72–85, Jan. 2019.
[51] D. Çelik and M. E. Meral, "A novel control strategy for grid connected distributed generation system to maximize power delivery capability," *Energy*, vol. 186, Nov. 2019, Art. no. 115850.
[52] T. Kauffmann, U. Karaagac, I. Kocar, S. Jensen, E. Farantatos, A. Haddadi, and J. Mahseredjian, "Short-circuit model for type-IV wind turbine generators with decoupled sequence control," *IEEE Trans. Power Del.*, vol. 34, no. 5, pp. 1998–2007, Oct. 2019.
[53] P. Mishra, A. K. Pradhan, and P. Bajpai, "Adaptive distance relaying for distribution lines connecting inverter-interfaced solar PV plant," *IEEE Trans. Ind. Electron.*, vol. 68, no. 3, pp. 2300–2309, Mar. 2021.

KUKKALA LIKHITHA received the B.Tech. degree in electrical and electronics engineering from the Visvesvaraya National Institute of Technology (VNIT), Nagpur, India, in 2018, and the M.Tech. degree in smart electric grid from the National Institute of Technology (NIT), Warangal, India, in 2022. She joined Hitachi Energy India Development Center, Bengaluru, in 2022, as a Research and Development Engineer. She is involved in the development of relay application function library (AFL) related to power system protection and monitoring. She has filed one patent. Her research interests include power system protection, monitoring applications, and renewable integration.

O. D. NAIDU (Senior Member, IEEE) received the Ph.D. degree from the Indian Institute of Technology (IIT) Kharagpur, Kharagpur, India. From 2009 to 2012, he was a Senior Power System Application Development Engineer with the ABB India Development Center, Bengaluru, India. From 2012 to 2019, he was a Principal Scientist with the ABB Corporate Research Center, Bengaluru. He is currently a Senior Principal Engineer with Hitachi Energy Research and Development Center, Bengaluru. He is the author of more than 50 scientific articles and 45 patent applications. He holds 15 granted patents. His research interests include power system protection, fault location, renewable integration and power system monitoring, and artificial intelligence applications to power system protection and monitoring. He was a recipient of the Young Innovator and Entrepreneur Award from the Indian National Academy of Engineering (INAE), for his contribution to the field of power system protection and monitoring.